Acta Materialia 119 (2016) 35–42

Contents lists available at ScienceDirect

Acta Materialia

journal homepage: www.elsevier.com/locate/actamat

Full length article

# Mechanical properties and optimization of the aging of a dilute Al-Sc-Er-Zr-Si alloy with a high Zr/Sc ratio

Anthony De Luca [a, b, *], David C. Dunand [a], David N. Seidman [a, b]

[a] Department of Materials Science and Engineering, Northwestern University, 2220 Campus Drive, Evanston, IL 60208-3108, USA
[b] Northwestern University Center for Atom-Probe Tomography, Northwestern University, 2220 Campus Drive, Evanston, IL 60208-3108, USA

ARTICLE INFO

*Article history:*
Received 17 June 2016
Accepted 7 August 2016
Available online 11 August 2016

*Keywords:*
Al-Sc-Er-Zr-Si alloy
Precipitation strengthening
High-temperature alloy
Mechanical properties
Microhardness

ABSTRACT

Precipitation strengthening behavior during aging of an Al-0.014Sc-0.008Er-0.08Zr-0.10Si (at.%) alloy was investigated utilizing microhardness, electrical conductivity and scanning electron microscopy. This new composition, with a Sc/Zr ratio (in at.%) smaller than 1/5 represents a significant reduction of the alloy's cost, when compared to more usual Al-0.06Sc (at.%) based alloys with typical Sc/Zr ratios of 3. The research presented herein focuses on identifying the optimal homogenization duration at 640 °C and additionally the temperature range at which a single-step aging treatment will achieve the highest possible microhardness in the shortest time. Due to a compromise between dissolution of Er-Si rich primary precipitates, homogenization of the Zr distribution and precipitation of large $Al_3Zr$ precipitates, 8 h at 640 °C appears to be the optimal homogenization duration for this alloy, leading to an hardness of 571 ± 22 MPa after aging for 24 h at 400 °C. To study the precipitation behavior of this *low-Sc concentration alloy*, isochronal aging to 575 °C with two different heating rates was performed. The small Sc concentration, compensated by a high Zr concentration, permits the alloy to achieve a similar peak microhardness during isochronal aging (587 ± 20 MPa) as the corresponding Sc-richer and Zr-leaner alloys. The isochronal aging experiments permits us to identify the best aging temperature as between 350 and 425 °C.



## 1. Introduction

The automotive industry has steadily reduced the environmental footprint of vehicles by making more efficient use of fuel. One way to achieve this goal is to decrease vehicle mass by an increased use of low-density aluminum alloys [1]. Those lightweight aluminum alloys are limited, however, to lower temperatures (below ~220 °C) due to the dissolution or phase transformation of their strengthening precipitates. To utilize aluminum alloys for high-temperature applications in the automotive and aerospace industries, one approach is to create coherent $L1_2$ precipitates containing slow-diffusing elements, which strengthen the alloy by impeding dislocation motion and which are stable and coarsen slowly by diffusion at the operating temperature [2].

Several slow-diffusing transition elements (M) form nanometric diameter $Al_3M$ ($L1_2$) precipitates when precipitated from a supersaturated aluminum solid-solution [2]; the most widely studied and least dense being Sc. Trace amounts of Sc increase drastically the strength of an Al alloy due to the formation of a high number density of nanometric $Al_3Sc$ ($L1_2$) precipitates coherent with the aluminum matrix. For example, a base aluminum microhardness of 200 MPa can be increased to 800 MPa by the addition of 0.18 at.% Sc [3,4]. Due to the relatively high diffusivity of Sc, only a few hours at 300–350 °C are needed to achieve optimal precipitation of coherent $Al_3Sc$ ($L1_2$) precipitates and reach peak microhardness. The alloy's long term use cannot, however, exceed ~300 °C due to the coarsening of $Al_3Sc$ precipitates [3,4].

Due to the small diffusivity of Zr in aluminum [2], precipitation strengthening of Al-Zr alloys is extremely sluggish, generally needing more than 100 h of aging to reach peak microhardness [5–10]. The metastable $Al_3Zr$ ($L1_2$) precipitates achieve relatively small number densities, so the strengthening effect is smaller than when using Sc, thus limiting usage of Al-Zr alloys. $Al_3Zr$ ($L1_2$) precipitates exhibit a higher coarsening resistance than $Al_3Sc$ ($L1_2$) precipitates. Alternatively, Er has a larger diffusivity than Sc [2,11], and thus $Al_3Er$ ($L1_2$) precipitates nucleate and grow at low

* Corresponding author. Department of Materials Science and Engineering, Northwestern University, 2220 Campus Drive, Evanston, IL 60208-3108, USA.
*E-mail address:* anthony.deluca@northwestern.edu (A. De Luca).

http://dx.doi.org/10.1016/j.actamat.2016.08.018
1359-6454/

temperatures and therefore Al-Er alloys suffer from an early loss of strength [12], preventing the use of Al-Er alloys for high-temperature applications. Due to the high lattice parameter mismatch between coherent $Al_3Er$ ($L1_2$) precipitates and the Al-matrix, those precipitates provide high creep-resistance to Al-Er alloys.

The addition of Sc and Zr or Sc and Er to aluminum results in the improvement of both base alloys. In Al-Sc-Zr alloys, the coherent $Al_3Sc$ ($L1_2$) precipitates that form during the early stage of aging acts as heterogeneous sites for precipitation of Zr, resulting in the formation of coherent core-shell $Al_3(Sc,Zr)$ ($L1_2$) precipitates, with the core enriched in Sc and the shell enriched in Zr [13–18]. Due to the formation of this Zr-rich shell, the precipitates' coarsening rate is reduced. Al-Sc-Er alloys behave similarly [19,20]; Er atoms form *nuclei* onto which the Sc atoms precipitate, forming an Er-rich core surrounded by a Sc-rich shell. In this case, the Sc-shell behaves similarly to the Zr-shell acted in the Al-Sc-Zr alloy, preventing fast coarsening of coherent $Al_3(Sc,Er)$ ($L1_2$) at elevated temperatures. The high number density of $Al_3Er$ *nuclei* are maintained during aging, permitting the attainment of higher volume fractions and thus increasing slightly the strength of the alloy at peak microhardness. Most importantly, the Er-rich core increases the lattice parameter mismatch of the precipitates with the Al-matrix, thereby increasing the creep resistance of the alloy [20].

The addition of Zr and Er to an Al-Sc alloy has the advantages of both ternary Al-based alloys [21]; Er promotes early nucleation of a high number density of precipitates with an increased lattice parameter mismatch, improving creep strength, while Zr decelerates the coarsening rate, thereby inducing a high temperature stability of the precipites. For example, a quaternary Al-0.05Sc-0.01Er-0.06Zr (at.%) alloy takes 30 min at 400 °C to reach a microhardness plateau of ~450 MPa, which is stable for at least 6 mon at this temperature [21]. The precipitates display a complex core-double shell structure, with an Er-enriched core, a Sc-rich inner shell and a Zr-rich outer shell. This core-double shell is a result of the differences in the diffusivities of the elements Er, Sc and Zr ($D_{Er} > D_{Sc} > D_{Zr}$), which is why they precipitate sequentially.

The strength of the quaternary Al-Sc-Zr-Er alloy can further be increased by a Si micro-addition [22–24]. Although Si doesn't form intermetallic compounds with Al, it forms M-Si-V clusters (M is a metal and V is a vacancy), which can diffuse faster than isolated M atoms in the α-Al matrix, thus allowing faster growth of the precipitates [25]. These clusters also act as *nuclei* for heterogeneous precipitation and increases the number density of precipitates and their volume fraction. For example, addition of 0.05 at.% Si to an Al-0.055Sc-0.005Er-0.02Zr (at.%) alloy increases the peak microhardness by 50 MPa, while reducing the aging heat treatment to 15 min [23]. Higher concentrations of Si further increase the alloy's strength [24]. Due to the enhanced solute diffusivity induced by silicon, the higher is the Si concentration the faster the precipitates coarsen. Atom-probe tomography (APT) experiments demonstrates that Si additions also modify the concentration profiles of the precipitates. The precipitates exhibit a Sc/Er/Si enriched core, Si being on the Al sub-lattice surrounded by a Zr-enriched shell instead of the core-double shell observed in Si-free alloys [23,24]. The mechanism underlying this structure are presently unclear, although it has been proposed to be due to either co-precipitation of $(Al,Si)_3(Sc,Er)$ or due to the homogenization of the core-shell structure during aging.

Attempts have been made to produce Sc-free Al-Er-Zr [26,27] and Al-Er-Zr-Si [28] alloys by increasing strongly the Er concentration (0.04 at.%) and the Zr concentration to 0.1 at.%. As shown by Wen et al. [26,27], the addition of Zr to Al-Er alloys decelerates the coarsening rate of the $Al_3Er$ precipitates due to the formation of a Zr-enriched shell. The Al-0.04Er-0.08Zr alloy reaches a peak microhardness of 540 MPa after 64 h of aging at 400 °C. Due, however, to the sluggish diffusion of Zr in the Al-matrix, the $Al_3Er$ precipitates experience early coarsening before the Zr-shell forms. There isn't isothermal aging data on Al-Er-Zr alloys with Si additions; it is, however, expected that Si accelerates the precipitation kinetics and causes stronger strengthening as observed for Al-Yb-Zr-Si alloys [29].

Although Sc-free Al-Er-Zr alloys are strong and inexpensive, the long aging times necessary to achieve peak microhardness is a major drawback. The objective of the present research is to adjust the concentrations of Sc, Zr and Si in Al-0.055Sc-0.005Er-0.02Zr-0.XY Si (at.%) alloys studied previously by Vo et al. [23,24], to minimize its Sc content, thereby lowering its price, while keeping the processing time as short as possible and maintaining good mechanical properties. We chose to use a small Sc concentration, rather than eliminating it, to prevent the early coarsening of $Al_3Er$ precipitates by either forming a Sc-enriched shell, or co-precipitating with Er, thereby forming $Al_3(Sc,Er)$ ($L1_2$) precipitates. We then compensate for the low Sc content by increasing the Zr concentration, while maintaining the Si content required to accelerate Zr precipitation. As compared to the previous Al-0.055Sc-0.005Er-0.02Zr-0.XY Si (at.%) alloys, the majority of the expensive Sc has been replaced by the much cheaper Zr, reducing the Sc content by a factor 4 (from 0.055 to 0.015 at.%), and increasing concomitantly the Zr content by the same factor (from 0.02 to 0.08 at.%). To avoid the rapid coarsening of precipitates due to the high Si concentration used previously [24], a relatively low Si concentration of 0.10 at.% is chosen. The Er concentration (0.005 at.%) remains unchanged. This article reports on the optimization of the homogenization step and the following precipitation strengthening behavior of the above noted *low-Sc concentration alloy* during isochronal aging.

### 1.1. Experimental procedures

The alloy with a nominal composition of Al-0.02Sc-0.005Er-0.08Zr-0.10Si at.% (Al-0.03Sc-0.03Er-0.27Zr-0.10Si wt.%), was melted in alumina crucibles in a resistively heated furnace by adding, to molten 99.99 at.% pure Al, appropriate concentrations of Al-8.0 wt% Zr, Al-2 wt.% Sc, Al-3.9 wt% Er master alloys preheated to 640 °C and Al-12.6 wt% Si preheated at 450 °C. The melt was maintained in air for 1 h at 800 °C to ensure full dissolution of the master alloys, regularly stirred, and then cast into a graphite mold. The mold was preheated to 200 °C and placed on an ice-cooled copper platen immediately before casting to enhance directional solidification. The chemical compositions of the as-cast alloy, sampled at the top and bottom positions in two separate ingots, was measured by direct current plasma mass spectroscopy (DCPMS) at ATI Wah Chang (Albany, OR), and the average results are presented in Table 1. No significant discrepancy was observed between the different samples and the iron concentration was less than the detection limit (<50 at ppm). APT was also utilized to measure alloy chemical composition, using the average values of ten specimens (cf. Table 1). The APT results are in reasonable agreement with the DCPMS measurements. However, when compared to the nominal

**Table 1**
Composition (at.%) of the investigated alloy, as measured by direct plasma emission spectroscopy (DCPMS) and local-electrode atom-probe (LEAP) tomography.

| | Sc | Er | Zr | Si |
|---|---|---|---|---|
| Nominal | 0.02 | 0.0045 | 0.08 | 0.10 |
| DCPMS | 0.014 | 0.0075 | 0.075 | 0.094 |
| LEAP | 0.013 | 0.0057 | 0.068 | 0.086* |

*Atomic concentration of $^{28}Si^{2+}$ ions in LEAP.

composition, the Sc concentration is lower. In the reminder of this article, we use the DCPMS composition of the alloy, Al-0.014Sc-0.008Er-0.08Zr-0.10Si at.%, and we express all compositions in atomic percent (at. %). For easier reading, and compared with other alloys, this alloy is denoted herein the "*low Sc alloy*".

To identify the best homogenization condition, the as-cast alloy was homogenized in air at 640 °C for times ranging between 0 and 24 h, followed by water quenching. Isochronal aging heat experiments was performed after homogenization, with steps of 25 °C for 1 or 3 h, starting at a temperature of 100 °C and through 575 °C. All aging treatments were performed in air and terminated by water quenching.

Vickers microhardness measurements were performed employing a Duramin-5 microhardness tester (Struers) utilizing an applied load of 200 g for 5 s on samples polished to at least a 1 μm surface finish. A minimum of ten and up to twenty indentations, in different grains, were made for each specimen. Electrical conductivity measurements were performed utilizing a Sigmatest 2.069 eddy current instrument (Foerster Instruments, Pittsburgh, PA) on the same $2 \times 2$ cm$^2$ sample subjected to cumulative heat-treatment steps. For each specimen, five measurements were performed at each frequencies 120, 240, 480, and 960 kHz. The as-cast and as-homogenized microstructures, on samples polished using a 0.06 μm colloidal silica suspension, was investigated using a Hitachi SU8030 scanning electron microscope (SEM), equipped with an Oxford X-max 80 mm detector for energy-dispersive x-ray spectroscopy (EDS) measurements, allowing us to detect primary precipitates and to estimate qualitatively their compositions. Following SEM observations, the samples where etched with Keller's reagent (95% water, 2.5% $HNO_3$, 1.5% HCl, 1% HF by volume) to reveal grain boundaries. The dendritic structure of the alloy was further revealed using Weck's reagent (100 mL water, 4 g $KMnO_4$ and 1 g NaOH).

## 2. Results

### 2.1. Minimization of homogenization time

Scanning electron microscope (SEM) observations of the as-cast state (Fig. 1a) revealed the presence of 1–2 μm primary Er- and Si-rich precipitates, with an areal density of ~200–500 mm$^{-2}$ and an estimated atomic composition ratio of Si:Er of 1.05 ± 0.15. The formation of these primary precipitates has been reported for Al-Sc-Er-Zr-Si alloys [23,24] and is due to the strong segregation of Er and Si, which occurs during solidification of the ingot upon casting [23,24]. No Zr-rich primary precipitates were observed. However, due to the incomplete dissolution of the Al-Zr master alloy in the melted alloy, a few $Al_3Zr$ flakes were detected (not shown). Their number density being very low – they were observed less than once across five $1 \times 1$ cm$^2$ samples – their impact on the measured properties of the alloy can therefore be neglected.

The cast alloy was homogenized at 640 °C for durations ranging from 1 to 24 h. The evolution of microhardness and electrical conductivity as a function of homogenization time are plotted in Fig. 4a and **b,** respectively. The alloy displays an as-cast microhardness of 245 ± 7 MPa. During the homogenization annealing, the microhardness increases to 266 ± 7 MPa after 4 h, before decreasing to 250 ± 7 MPa after 24 h. This small increase in microhardness implies that some precipitation may be occurring during homogenization. The monitoring of electrical conductivity confirms this hypothesis. The electrical conductivity data displays increasing conductivity as the homogenization time increases, from ~30.10 MS m$^{-1}$ in the as-cast state to ~31.05 MS m$^{-1}$ after 24 h of aging. This continuous increase of electrical conductivity indicates that atoms are precipitating out of the supersaturated solid solution as soon as the homogenization annealing commences.

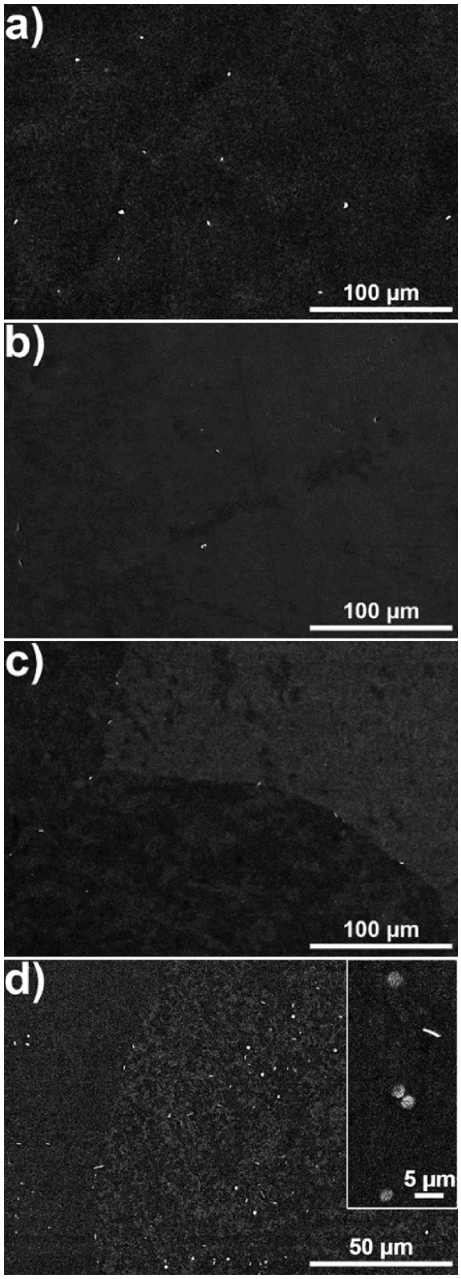


**Fig. 1.** SEM micrograph of the *low-Sc alloy* (a) in as cast state, showing a high number density of Er- and Si- rich primary precipitates, and (b–d) after homogenization at 640 °C for 2, 8 and 24 h, respectively. (b) After 2 h of aging, primary Er- and Si- rich precipitates are infrequently observed. (c) For longer aging durations, $Al_3Zr$ rod-like precipitates form at grain boundaries (c). (d) Only samples aged for 24 h display a high number density of $Al_3Zr$ rod- and platelet-like precipitates inside grains.

Although not detectable from the electrical conductivity evolution, the Er- and Si-rich precipitates visible in Fig. 1a are dissolving during the first hours, with only a few of them being observed after 2 h of homogenization (Fig. 1b). For samples aged longer than 2 h, no Er- and Si-rich precipitates were ever observed; however, a low volume fraction of grain boundary $Al_3Zr$ rod-like precipitates, with a length of ~3 μm, were identified (Fig. 1c). In addition to these grain boundary precipitates, samples aged for 24 h exhibit a high number density of intra-granular rod- and platelet-like $Al_3Zr$ precipitates (Fig. 1d). The increase of

electrical conductivity during homogenization annealing can thus be explained by the precipitation of Zr, which is undesirable, as it leads to a loss of solute for strengthening during subsequent aging. Post-SEM etching of the samples with Keller's etchant (Fig. 2) revealed that the alloy has millimeter diameter grains, which are retained during the homogenization annealing; large grain diameters are preferred to obtain good creep resistance. Further etching with Weck's reagent revealed a dendritic structure within the grains, Fig. 3, for post casting samples, and after homogenization for 2 h. In the as-cast conditions, the etchant revealed a well-defined cell structure, with a 20–30 μm core and ~4 μm wide inter-dendritic channels. After 1 h of aging at 640 °C, the dendritic structure evolved to a larger cell diameters (>35 μm) and ~15 μm widths and more diffuse channels. Although homogenization annealing appears to have an effect on the dendritic structure in the alloy, further modification did not occur, preventing complete homogenization of solute even after 24 h, only leading to the previously mentioned intradendritic $Al_3Zr$ precipitates.

To determine the best compromise between dissolution of the Er/Si-rich primary precipitates and loss of solute due to Zr precipitation, samples were homogenized for durations up to 24 h and then aged at 400 °C for 24 h, which is the time needed to reach peak hardness at 400 °C for this *low-Sc concentration alloy* [30]. The associated microhardness and electrical conductivity curves are displayed in Fig. 4a and b, respectively. After this aging step, a significant difference in microhardness can be observed between samples without an homogenization treatment (455 ± 26 MPa) and with an optimal homogenization treatment of 8 h (571 ± 22 MPa). For longer homogenization times of 16 or 24 h, the peak microhardness is smaller (538 ± 20 MPa). This ~6% drop is most probably due to the smaller concentration of Zr available for precipitation hardening after too long an homogenization time, where Zr precipitates from solution in the form of micron-diameter precipitates, which are too large to affect the microhardness. Although it is possible that the increased microhardness, which was obtained for the sample aged 8 h, could be due to some local composition inhomogeneity; this higher microhardness was observed anew during isochronal aging of samples homogenized for either 8 h or 24 h (Fig. 5c).

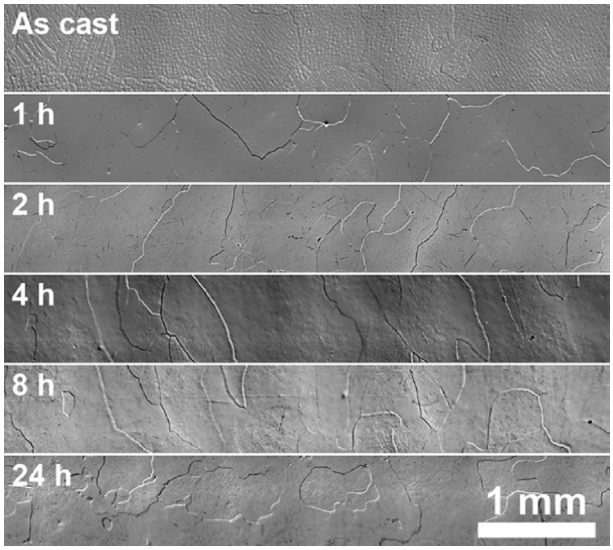


**Fig. 2.** Optical micrograph of the *low-Sc alloy* in the as cast state, or homogenized at 640 °C between 1 and 24 h. The grain boundaries were revealed using Keller's reagent.

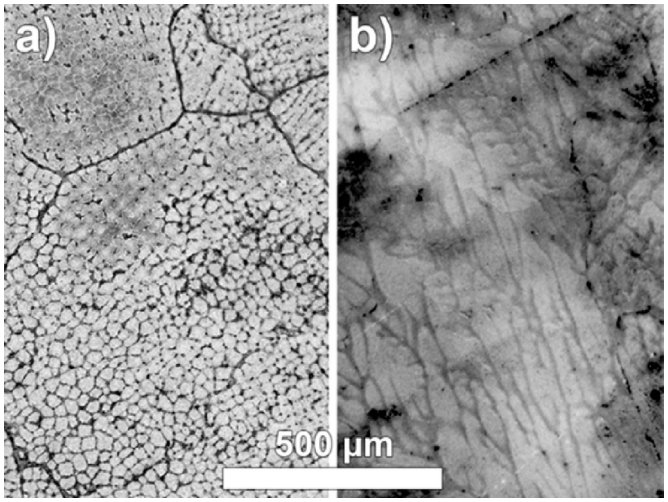


**Fig. 3.** (a) Optical micrograph of the *low-Sc alloy* in as cast state and (b) after homogenization at 640 °C for 2 h. The dendritic structure was revealed using Weck's reagent.

### 2.2. Isochronal aging

The temporal evolution of the Vickers microhardnesses and electrical conductivities during isochronal aging, of our alloy (denoted as *low-Sc alloy)*, either homogenized for 8 h or 24 h, are

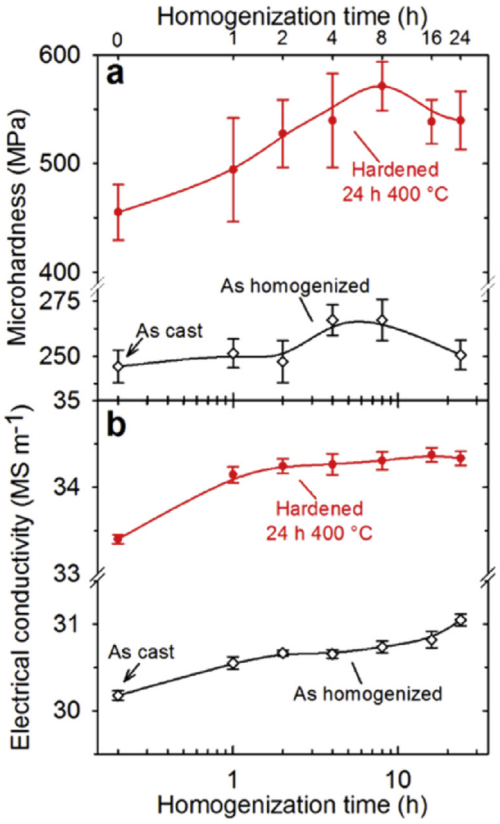


**Fig. 4.** Evolution of (a) Vickers microhardness and (b) electrical conductivity, during homogenization annealing of the *low-Sc alloy* at 640 °C (empty diamonds) and after a subsequent hardening aging step at 400 °C for 24 h (solid red dots). (For interpretation of the references to colour in this figure legend, the reader is referred to the web version of this article.)

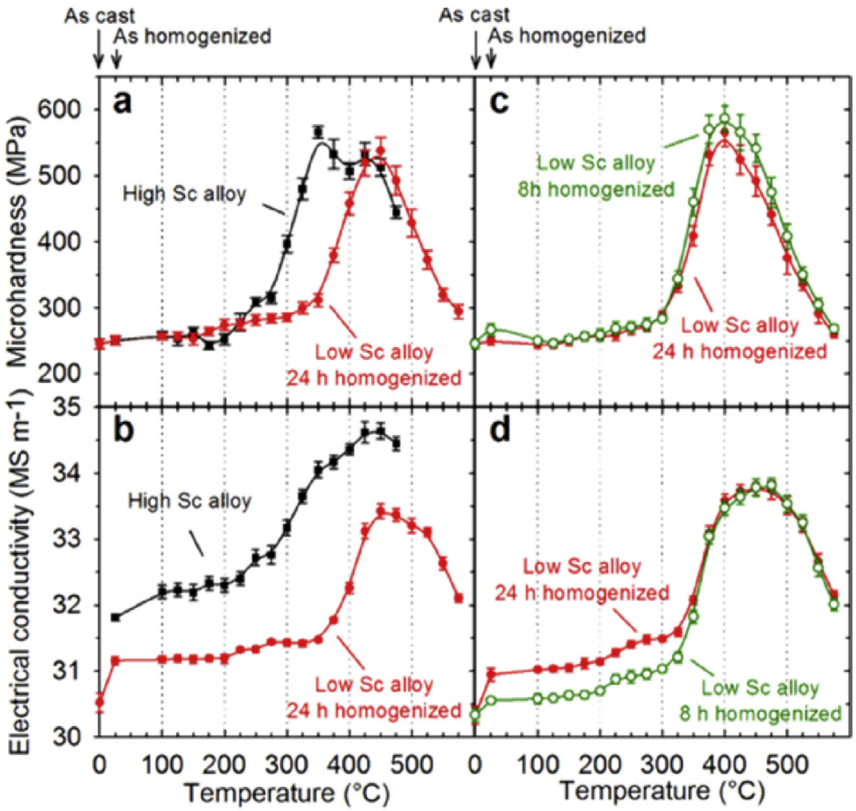


**Fig. 5.** Evolution of Vickers microhardness and electrical conductivity during isochronal aging, with steps of 25 °C for 1 h (a, b) or 3 h (c, d), for Al-0.055Sc-0.005Er-0.02Zr-0.05Si at.% (*high-Sc alloy*) [23] homogenized at 640 °C for 2 h (black squares), and Al-0.014Sc-0.008Er-0.08Zr-0.1Si at.% (*low-Sc alloy*) homogenized at 640 °C for 8 h (green circles) or 24 h (solid red dots). (For interpretation of the references to colour in this figure legend, the reader is referred to the web version of this article.)

displayed in Fig. 5. Data from the Al-0.055Sc-0.005Er-0.02Zr-0.05Si alloy previously studied by Vo et al. [23] (denoted as *high-Sc alloy*), homogenized 2 h and then aged isochronally with steps of 25 °C for 1 h, are presented for comparison in Fig. 5a and b.

In the *high-Sc alloy*, precipitation commenced in the temperature range 225–275 °C, causing an increase of conductivity and microhardness from 252 ± 8 MPa to 315 ± 8 MPa. This change in microhardness is attributed to Er precipitating from solution and forming $Al_3Er$ precipitates, Er having a larger diffusivity than Sc and Zr [23]. At temperatures higher than 275 °C, Sc precipitates on the previously formed $Al_3Er$ *nuclei* [23], which causes a significant increase of the microhardness, peaking at 566 ± 9 MPa at 350 °C. The microhardness then decreases with increasing temperature due to coarsening, before peaking again at 425 °C at a value of 532 ± 18 MPa, the latter peak is attributed to Zr precipitation [23]. Above 450 °C (~0.78 of the absolute melting point of Al), both the electrical conductivity and microhardness values decrease continuously, indicating that the precipitates are both dissolving and coarsening.

Data from the 1 h step isochronal aging of the *low-Sc alloy*, homogenized 24 h, are displayed in Fig. 5a and b. Although a small increase of the electrical conductivity is noticeable at 225 °C, which corresponds to the temperature where Er is anticipated to precipitate, the microhardness does not abruptly change, unlike the *high-Sc alloy*, but increases progressively from 251 ± 7 MPa after homogenization, to 285 ± 6 MPa at 300 °C. Due to the small concentration of Sc in this alloy, it appears that precipitation of this element only increases the microhardness by ~25 MPa between samples aged isochronally to 300° and to 350 °C; this later temperature corresponding to the peak temperature for the *high-Sc alloy*. For the *low-Sc alloy*, at temperatures greater than 350 °C, the diffusivity of Zr becomes sufficiently large to permit significant diffusion and precipitation of this solute element on previously formed $Al_3(Sc,Er)$ precipitates. The microhardness and electrical conductivity increases continuously and peaks at 450 °C, with a value of 538 ± 20 MPa. Taking into account the 6% higher microhardness for samples homogenized for 8 h, the optimized peak microhardness should be ~568 MPa, which is the same peak microhardness that is achieved by the *high-Sc alloy*. At 475 °C, although the electrical conductivity is the same as at 450 °C, the microhardness is decreasing, which indicates precipitate coarsening. At higher temperatures the electrical conductivity decreases, which indicates precipitate dissolution, thereby explaining the rapid decrease of the microhardness.

Data from the 3 h step isochronal aging of the *low-Sc alloy*, homogenized for 8 or 24 h, are displayed in Fig. 5c and d. For both homogenization conditions, the evolution of microhardness and electrical conductivity follow similar trends; the major differences are the initial electrical conductivity and peak microhardness values. At temperatures lower than 300 °C, the microhardness and electrical conductivity values slowly but steadily increase with the aging temperature. At 300 °C, a microhardness of 286 ± 6 MPa is obtained for both homogenization conditions. The longer aging time (3 h) permits Zr atoms to diffuse longer distances, when compared with the 1 h isochronal aging step, Fig. 5a, the microhardness and electrical conductivity increases associated with Zr precipitation are shifted by 50 °C toward lower temperatures, and thus happens at 325 rather than 375 °C. The microhardness, Fig. 5c, then increases sharply and peaks at 400 °C. The peak microhardness values for the *low-Sc alloy* homogenized 8 or 24 h at 640 °C are 587 ± 20 MPa and 566 ± 21 MPa, respectively. At higher

temperatures the microhardness first decreases due to precipitate coarsening, since no change in electrical conductivity is observed up to 475 °C. At higher temperatures the electrical conductivity decreases, which indicates again that precipitates are dissolving. Based on these observations, the optimal aging temperatures for the *low-Sc alloy* are anticipated to lie between 350 and 425 °C.

## 3. Discussion

### 3.1. Optimization of homogenization time

The main goal of the homogenization heat treatments is to dissolve the primary precipitates that form during casting, and also to reduce the concentration gradients resulting from dendritic solidification. Although the sum of the Er, Sc and Zr concentrations in this *low-Sc alloy* is high (0.0965%), no primary $Al_3Zr$ or $Al_3Sc$ precipitates were observed. A high number density of Er- and Si-rich primary precipitates in the as-cast samples is, however, detected, Fig. 1a. Because they sequester Er and Si atoms these primary precipitates not only reduce the number of Er atoms available for subsequent precipitation strengthening on aging, but they also prevent Si atoms from enhancing the diffusion kinetics of other solute atoms [25]. Aging of a non-homogenized alloy thus induces a comparatively small strengthening increment, Fig. 4a. A heat treatment of 2–4 h is necessary to dissolve the primary precipitates, Fig. 1b and c. As demonstrated in previous research on Al-Sc-Er-Zr-Si alloys, the dissolution of $Al_3Er$ precipitates can be monitored by measuring the electrical conductivity during homogenization [23,24]. Dissolution of precipitates releases solute atoms into the matrix, thereby reducing its electrical conductivity [23,24]. The electrical conductivity doesn't, however, decrease during homogenization, Fig. 4b, but rather it increases continuously, even after 24 h at 640 °C. SEM observations reveal precipitation of Zr into $Al_3Zr$ precipitates during homogenization. Initially absent, $Al_3Zr$ precipitates become easily observable at grain boundaries after 4 h, Fig. 1c, and within grains after 24 h of homogenization, as large platelet- or rod-like precipitates, Fig. 1d. Due to the peritectic solidification of Al-Zr alloys, the Zr atoms segregate at the dendrite cores during solidification. The Zr concentration in these regions thus exceeds the solid-solubility of 0.067 at.% at 640 °C [31], and therefore homogenization annealing induces precipitation. It was previously demonstrated that homogenization of Al-Zr alloys could be detrimental to further precipitation hardening due to a major loss of solute [32]. For that reason, Zr-rich alloys are usually not homogenized before precipitation aging [6,7,17,18]. In the case of the *low-Sc alloy*, the achievable peak microhardness after aging at 400 °C increases with longer homogenization times, Fig. 4a, peaking for 8 h of homogenization.

The increased microhardness for samples homogenized for up to 4 h can be explained by the dissolution of Er atoms from the primary precipitates, which effectively compensates for the loss of Zr in solid-solution via precipitation of coarse $Al_3Zr$ precipitates. The highest microhardness is achieved for 8 h of homogenization and it decreases for longer aging times. This additional increase of microhardness compared to 4 h cannot be accounted for by dissolution of $Al_3Er$ precipitates as no primary precipitates were detected in samples homogenized for 4 h. Silicon atoms may enhance the diffusivities of Er, Sc or Zr in the α-Al matrix [25], hence it is possible that the high concentration of Si in this alloy permits some homogenization of the Zr dendritic microstructure.

In conclusion, homogenization of this alloy is necessary to achieve higher microhardness values after a subsequent aging step. The optimum aging duration has been identified, allowing an increase in the achievable peak microhardness. Compared, however, to the previous Al-Sc-Er-Zr-Si alloys with lower Zr and higher Sc concentrations, the homogenization times have been increased from 0.5 to 2 h [23,24] to 8 h at 640 °C. This longer homogenization time is considered acceptable within an industrial environment.

### 3.2. Effective activation energy for precipitation

The electrical conductivity of a material is affected by strong scattering of electrons by point defects in the matrix, and to a smaller extent by the presence of precipitates. Thus following the change in electrical conductivity or inversely its electrical resistivity, ρ, Fig. 6a, thereby monitoring the change in the matrix's composition and the precipitation process. At a low defect concentration, the increase in resistivity is proportional to the concentration of impurities. For example, in the case of Sc in aluminum, the electrical resistivity ρ increases by 34 nΩ-m per atomic % [33]. Due to the presence of four impurity species in our alloy – Sc, Er, Zr and Si — each displaying a different electron scattering, it is not possible to monitor precisely the change in matrix composition from electrical conductivity curves and obtain solubility limits. Analyzing such curves can, however, permit to extract the apparent activation energy for precipitation [34].

In our case, due to the close spacing between the annealing temperatures, we can approximate the isochronal aging curves as annealing curves with a constant heating rate. By performing two annealing experiments, utilizing two different heating rates, $\alpha_1$ and $\alpha_2$, one can obtain an apparent activation energy using the following equation [34]:

$$\ln\left(\frac{\alpha_2 T_1^2}{\alpha_1 T_2^2}\right) = \frac{Q}{k_B}\left(\frac{1}{T_1} - \frac{1}{T_2}\right) \quad (1)$$

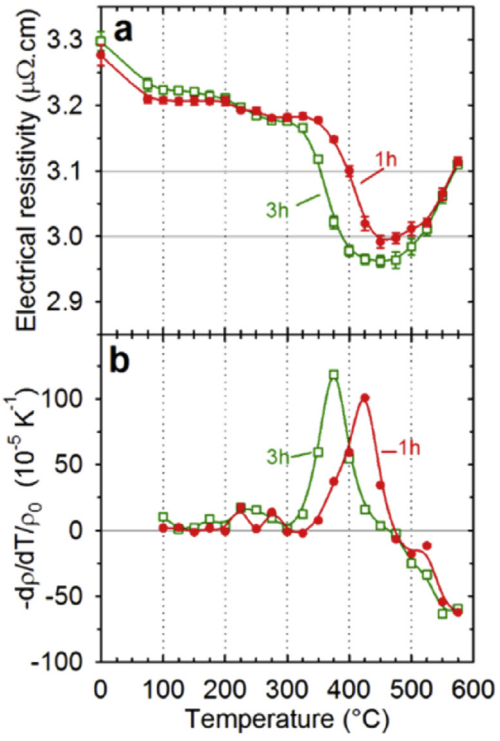


**Fig. 6.** (a) Evolution of electrical resistivity during isochronal aging with steps of 25 °C for 1 h (solid red dots) or 3 h (green squares) for the *low Sc alloy*, homogenized at 640 °C for 24 h. (b) Negative numerical derivatives of the measured resistivity during isochronal aging of the *low Sc alloy* divided by the initial resistivity, $\rho_0$. (For interpretation of the references to colour in this figure legend, the reader is referred to the web version of this article.)

where $T_1$ and $T_2$ are the temperatures at which identical values of ρ are achieved for the heating rates $\alpha_1$ and $\alpha_2$, respectively, where $k_B$ is Boltzmann's constant and T is the temperature in Kelvin. The apparent activation energy, Q, is obtained from Equation (1). Using the resistivity curves, Fig. 6a, an apparent activation energy of 0.70 ± 0.09 eV is obtained in the region where ρ increases linearly with T, between 3 and 3.1 μΩ-cm. The calculated apparent activation energy is small compared to the activation energies for diffusion of Sc or Zr in Al, 1.79 and 2.51 eV, respectively [2].

Another approach for determining the activation energy from isochronal aging experiments is to plot the negative numerical derivatives of the resistivity [35], Fig. 6b. This permits identifying the specific temperatures at which the rate of change of resistivity is the fastest for a given heating rate, permitting one to measure an activation energy using Equation (1), but also allowing one to identify more readily the temperature range for which an isothermal aging experiment will be optimal, in terms of duration and achievable microhardness. For the *low-Sc alloy*, the optimal aging temperature is between 350 and 425 °C. The apparent activation energy estimated using this method is 0.74 ± 0.11 eV.

Prior research on a binary Al-0.15Sc [33] and ternary Al-0.14Sc-0.04Zr alloys [35] reported small apparent activation energies for precipitation, in comparison to the activation energies for Sc diffusion in these alloys, 1.29 and 1.24 eV. The apparent activation energy we obtain is about one-half those values. No research has been reported on the effects of Er and Si on the apparent activation energy for precipitation. Since Er and Si increase the number density of *nuclei* [9,36], and Si enhances the diffusivities of Sc and Zr in the matrix by forming and diffusing as a Si-V-Zr trimer, with a smaller activation energy [25].

## 4. Conclusions

The properties of a low-Sc, high-Zr aluminum alloy, Al-0.015Sc-0.0045Er-0.08Zr-0.10Si at.%, designed to minimize the concentration of the most expensive element, Sc, while maintaining the desirable strengthening provided by precipitation of coherent $L1_2$ tri-aluminide precipitates, were investigated utilizing microhardness, electrical conductivity measurements, and observations by SEM. Based on the experimental results obtained, we conclude that reducing the cost of Al-Sc-Er-Zr-Si alloys can be achieved by replacing the expensive element Sc by the much less expensive element Zr, maintaining *only one-quarter of the original Sc concentration*, and compensating for this change by increasing the Zr concentration by a factor of four. Specifically, the following conclusions are deduced from the experimental results:

1. Primary Er- and Si-rich precipitates form during solidification of our newest Al alloy. At least 2 h of homogenization at 640 °C is necessary to dissolve precipitates and increase the Er supersaturation in the Al-matrix. No primary $Al_3Zr$ ($L1_2$) precipitates are observed after solidification. However, μm long rod- and platelet-like $Al_3Zr$ precipitates appear upon homogenization beyond 4 h. Homogenizing for 8 h permits the alloy to reach its highest peak microhardness upon subsequent aging. This optimum homogenization treatment reflects a compromise between homogenization of Er, Si and Zr solute elements, and early precipitation of $Al_3Zr$ in the dendrite cores.
2. During an isochronal aging with 1 h steps, the new alloy achieves a similar peak microhardness as the more expensive Sc-rich alloy, but with an upwards shift of 50 °C toward higher temperatures, indicating a slower precipitation kinetics.
3. Based on electrical conductivity measurements during isochronal aging experiments, the precipitates are anticipated to be stable for temperatures up to 475 °C, which represent an increase of 25 °C compared to our previous Sc-rich Al-Sc-Er-Zr-Si alloys.
4. Based on isochronal aging experiments, the optimal aging temperature that would permit achieving a high microhardness in the least amount of time is anticipated to be in the range 350–425 °C range.
5. An apparent activation energy for precipitation was determined utilizing two different heating rates during isochronal aging experiments. A value of 0.70 ± 0.09 eV/atom was calculated, which is smaller than the activation energies for diffusion of Sc or Zr in Al.
6. The formation and diffusion of Si-V-M trimers, with M being Sc, Er or Zr, is expected to be the underlying mechanism behind the calculated low activation energy

## Acknowledgments

This research was sponsored by the Ford-Northwestern University Alliance. APT was performed at the Northwestern University Center for Atom-Probe Tomography (NUCAPT). The local-electrode atom-probe tomograph at NUCAPT was acquired and upgraded with equipment grants from the MRI program of the National Science Foundation (NSF DMR-0420532) and the DURIP program of the Office of Naval Research (N00014-0400798, N00014-0610539, N00014-0910781). NUCAPT received support from the MRSEC program (NSF DMR-1121262) at the Materials Research Center, SHyNE Resource (NSF NNCI-1542205), and the Initiative for Sustainability and Energy at Northwestern (ISEN). This research made use of the EPIC facility (NU*ANCE* Center-Northwestern University), which receives support from the MRSEC program (NSF DMR-1121262) at the Materials Research Center; the International Institute for Nanotechnology (IIN); and the State of Illinois, through the IIN. The authors also gratefully acknowledge the Initiative for Sustainability and Energy at Northwestern (ISEN) for grants to upgrade the capabilities of NUCAPT. The authors kindly thank Drs. J. Boileau and B. Ghaffari (Ford) for numerous useful discussions.

## References

[1] P.K. Mallick, Materials, Design and Manufacturing for Lightweight Vehicles, CRC Press, Woodhead, Boca Raton, Oxford, 2010.
[2] K.E. Knipling, D.C. Dunand, D.N. Seidman, Criteria for developing castable, creep-resistant aluminum-based alloys – a review, Z. Für Met. 97 (2006) 246–265, http://dx.doi.org/10.3139/146.101249.
[3] E. Marquis, D.N. Seidman, Nanoscale structural evolution of $Al_3Sc$ precipitates in Al(Sc) alloys, Acta Mater 49 (2001) 1909–1919, http://dx.doi.org/10.1016/S1359-6454(01)00116-1.
[4] D.N. Seidman, E.A. Marquis, D.C. Dunand, Precipitation strengthening at ambient and elevated temperatures of heat-treatable Al(Sc) alloys, Acta Mater 50 (2002) 4021–4035, http://dx.doi.org/10.1016/S1359-6454(02)00201-X.
[5] E. Nes, Precipitation of the metastable cubic $Al_3Zr$-phase in subperitectic Al-Zr alloys, Acta Metall. 20 (1972) 499–506, http://dx.doi.org/10.1016/0001-6160(72)90005-3.
[6] K.E. Knipling, D.C. Dunand, D.N. Seidman, Nucleation and precipitation strengthening in dilute Al-Ti and Al-Zr alloys, Metall. Mater. Trans. A 38 (2007) 2552–2563, http://dx.doi.org/10.1007/s11661-007-9283-6.
[7] K.E. Knipling, D.C. Dunand, D.N. Seidman, Precipitation evolution in Al–Zr and Al–Zr–Ti alloys during isothermal aging at 375–425°C, Acta Mater 56 (2008) 114–127, http://dx.doi.org/10.1016/j.actamat.2007.09.004.
[8] K.E. Knipling, D.C. Dunand, D.N. Seidman, Precipitation evolution in Al–Zr and Al–Zr–Ti alloys during aging at 450–600°C, Acta Mater 56 (2008) 1182–1195, http://dx.doi.org/10.1016/j.actamat.2007.11.011.
[9] H. Li, J. Bin, J. Liu, Z. Gao, X. Lu, Precipitation evolution and coarsening resistance at 400°C of Al microalloyed with Zr and Er, Scr, Mater 67 (2012) 73–76, http://dx.doi.org/10.1016/j.scriptamat.2012.03.026.
[10] E. Çadirli, H. Tecer, M. Şahin, E. Yilmaz, T. Kirindi, M. Gündüz, Effect of heat treatments on the microhardness and tensile strength of Al–0.25wt.% Zr alloy, J. Alloys Compd. 632 (2015) 229–237, http://dx.doi.org/10.1016/j.jallcom.2015.01.193.
[11] M.E. van Dalen, R.A. Karnesky, J.R. Cabotaje, D.C. Dunand, D.N. Seidman, Erbium and ytterbium solubilities and diffusivities in aluminum as

determined by nanoscale characterization of precipitates, Acta Mater 57 (2009) 4081–4089, http://dx.doi.org/10.1016/j.actamat.2009.05.007.
[12] Y. Zhang, K. Gao, S. Wen, H. Huang, Z. Nie, D. Zhou, The study on the coarsening process and precipitation strengthening of $Al_3Er$ precipitate in Al–Er binary alloy, J. Alloys Compd. 610 (2014) 27–34, http://dx.doi.org/10.1016/j.jallcom.2014.04.093.
[13] C.B. Fuller, D.N. Seidman, D.C. Dunand, Mechanical properties of Al(Sc,Zr) alloys at ambient and elevated temperatures, Acta Mater 51 (2003) 4803–4814, http://dx.doi.org/10.1016/S1359-6454(03)00320-3.
[14] C. Fuller, J. Murray, D.N. Seidman, Temporal evolution of the nanostructure of Al(Sc,Zr) alloys: Part I – chemical compositions of Al(ScZr) precipitates, Acta Mater 53 (2005) 5401–5413, http://dx.doi.org/10.1016/j.actamat.2005.08.016.
[15] C. Fuller, D.N. Seidman, Temporal evolution of the nanostructure of Al(Sc,Zr) alloys: Part II-coarsening of Al(ScZr) precipitates, Acta Mater 53 (2005) 5415–5428, http://dx.doi.org/10.1016/j.actamat.2005.08.015.
[16] A. Deschamps, L. Lae, P. Guyot, In situ small-angle scattering study of the precipitation kinetics in an Al–Zr–Sc alloy, Acta Mater 55 (2007) 2775–2783, http://dx.doi.org/10.1016/j.actamat.2006.12.015.
[17] K.E. Knipling, R.A. Karnesky, C.P. Lee, D.C. Dunand, D.N. Seidman, Precipitation evolution in Al–0.1Sc, Al–0.1Zr and Al–0.1Sc–0.1Zr (at.%) alloys during isochronal aging, Acta Mater 58 (2010) 5184–5195, http://dx.doi.org/10.1016/j.actamat.2010.05.054.
[18] K.E. Knipling, D.N. Seidman, D.C. Dunand, Ambient- and high-temperature mechanical properties of isochronally aged Al–0.06Sc, Al–0.06Zr and Al–0.06Sc–0.06Zr (at.%) alloys, Acta Mater 59 (2011) 943–954, http://dx.doi.org/10.1016/j.actamat.2010.10.017.
[19] R.A. Karnesky, M.E. van Dalen, D.C. Dunand, D.N. Seidman, Effects of substituting rare-earth elements for scandium in a precipitation-strengthened Al–0.08 at. %Sc alloy, Scr. Mater 55 (2006) 437–440, http://dx.doi.org/10.1016/j.scriptamat.2006.05.021.
[20] R.A. Karnesky, D.N. Seidman, D.C. Dunand, Creep of Al-Sc microalloys with rare-earth element additions, Mater. Sci. Forum. 519–521 (2006) 1035–1040, http://dx.doi.org/10.4028/www.scientific.net/MSF.519-521.1035.
[21] C. Booth-Morrison, D.C. Dunand, D.N. Seidman, Coarsening resistance at 400°C of precipitation-strengthened Al–Zr–Sc–Er alloys, Acta Mater 59 (2011) 7029–7042, http://dx.doi.org/10.1016/j.actamat.2011.07.057.
[22] C. Booth-Morrison, D.N. Seidman, D.C. Dunand, Effect of Er additions on ambient and high-temperature strength of precipitation-strengthened Al–Zr–Sc–Si alloys, Acta Mater 60 (2012) 3643–3654, http://dx.doi.org/10.1016/j.actamat.2012.02.030.
[23] N.Q. Vo, D.C. Dunand, D.N. Seidman, Improving aging and creep resistance in a dilute Al–Sc alloy by microalloying with Si, Zr and Er, Acta Mater 63 (2014) 73–85, http://dx.doi.org/10.1016/j.actamat.2013.10.008.
[24] N.Q. Vo, D.C. Dunand, D.N. Seidman, Role of silicon in the precipitation kinetics of dilute Al-Zr-Sc-Er alloys, (To be submitted).
[25] C. Booth-Morrison, Z. Mao, M. Diaz, D.C. Dunand, C. Wolverton, D.N. Seidman, Role of silicon in accelerating the nucleation of $Al_3$(Sc,Zr) precipitates in dilute Al–Sc–Zr alloys, Acta Mater 60 (2012) 4740–4752, http://dx.doi.org/10.1016/j.actamat.2012.05.036.
[26] S.P. Wen, K.Y. Gao, Y. Li, H. Huang, Z.R. Nie, Synergetic effect of Er and Zr on the precipitation hardening of Al–Er–Zr alloy, Scr. Mater 65 (2011) 592–595, http://dx.doi.org/10.1016/j.scriptamat.2011.06.033.
[27] S.P. Wen, K.Y. Gao, H. Huang, W. Wang, Z.R. Nie, Precipitation evolution in Al–Er–Zr alloys during aging at elevated temperature, J. Alloys Compd. 574 (2013) 92–97, http://dx.doi.org/10.1016/j.jallcom.2013.03.237.
[28] N.Q. Vo, D.N. Seidman, D.C. Dunand, Aluminum Superalloys for Use in High Temperature Applications, 03/12/2015. Patent US20150259773.
[29] S.P. Wen, K.Y. Gao, H. Huang, W. Wang, Z.R. Nie, Role of Yb and Si on the precipitation hardening and recrystallization of dilute Al–Zr alloys, J. Alloys Compd. 599 (2014) 65–70, http://dx.doi.org/10.1016/j.jallcom.2014.02.065.
[30] A. De Luca, D.C. Dunand, D.N. Seidman, Coarsening resistance and mechanical properties of a dilute Al-Sc-Er-Zr-Si alloy with high Zr/Sc ratio, (to be submitted).
[31] H. Okamoto, Al-Zr (Aluminum-Zirconium), J. Phase Equilibria 23 (2002) 455–456, http://dx.doi.org/10.1361/105497102770331497.
[32] K.E. Knipling, Development of a Nanoscale Precipitation-strengthened Creep-resistant Aluminum Alloy Containing Trialuminide Precipitates, Northwestern University, 2006.
[33] H.-H. Jo, S.-I. Fujikawa, Kinetics of precipitation in $Al_3Sc$ alloys and low temperature solid solubility of scandium in aluminium studied by electrical resistivity measurements, Mater. Sci. Eng. A 171 (1993) 151–161, http://dx.doi.org/10.1016/0921-5093(93)90401-Y.
[34] A.C. Damask, G.J. Dienes, Point defects in Metals, Gordon and breach, New York, London, 1963.
[35] M. Vlach, I. Stulíková, B. Smola, N. Žaludová, J. Černá, Phase transformations in isochronally annealed mould-cast and cold-rolled Al–Sc–Zr-based alloy, J. Alloys Compd. 492 (2010) 143–148, http://dx.doi.org/10.1016/j.jallcom.2009.11.126.
[36] R.A. Karnesky, D.C. Dunand, D.N. Seidman, Evolution of nanoscale precipitates in Al microalloyed with Sc and Er, Acta Mater 57 (2009) 4022–4031, http://dx.doi.org/10.1016/j.actamat.2009.04.034.